CSCE Annual Conference

Growing with youth – Croître avec les jeunes

Laval (Greater Montreal)

June 12 - 15, 2019

THE EFFECT OF THE NON-COHESIVE HOMOGENOUS EMBANKMENT GEOMETRY ON THE BREACH OUTFLOW AND EROSION RATES DURING OVERTOPPING

Rahman, A.[1,1] , Nistor, I.[1,2], Infante, J-A.[1,3]
[1] Department of Civil Engineering, University of Ottawa, Ottawa, Ontario, Canada
[1] amanjrahman@uottawa.ca , [2] inistor@uottawa.ca , [3] jinfante@uottawa.ca

Abstract: The paper presents the results of a comprehensive experimental program conducted to obtain the effect of downstream slope on the planar breaching progress and outflow hydrograph of homogenous non-cohesive embankments due to overtopping. Visualizing flow by injecting fluorescent dye and using LED UV blacklight under controlled room conditions combined with high-speed cameras provided high-accuracy data of high temporal and spatial resolution of the processes investigated. Downstream slopes of (1:2, 1:3 and 1:4) were tested with the initial overtopping head of 0.05 and 0.10 m. The time-history of the pore-water-pressure (PWP) during overtopping flow on the downstream embankment face were recorded using micro-tensiometer-transducer probe assemblies (MTTPA). Styrofoam balls (2-3) mm size sprayed with fluorescent paint were used as tracers to measure flow surface velocity, in combinations with a high-speed Phantom 410L (HSPC) camera with a recording capacity of 1000 fps. The image processing and tracking particles velocity were achieved using the Davis@ commercial software. The element of novelty of this work is related to the deployment of recent technology and image processing tools which ensured the use of particle tracking velocimetry (PTV) in measuring the overtopping flow hydrograph. The hydrographs computed for the three embankment configurations indicated that the erosion rate for the steeper slope under the high initial overtopping head is relatively rapid due to the high acceleration of flow and the subsequent high shear stress applied on the bed material. In contrast, with a low initial overtopping head (5 cm), the downstream slope had a lesser impact on peak-flow.

1 INTRODUCTION

Dikes and earthen embankments are significant hydraulic infrastructure since ancient times and have played an essential role in the development of civilizations over many centuries. However, recent frequent flooding events because of the failure of those structures show the massive destructive hazard that can affect the communities located on the downstream side of the dams. The improvement of physical models for such phenomena is significant for hydraulic engineers and researchers to understand the detailed processes and predictions of such breach events. Moreover, accurate measurements are essential for validating flood and breach numerical models, for determining the spatial and temporal extent of inundation, and the emergency and mitigation plans for evacuation (Rifai et al. 2017).

Breaching of earthen embankments can occur in different ways mainly due to their overtopping, through piping or slope failure. However, the most common type of failure is due to overtopping (Zhang, et al. 2016).

Insufficient spillway capacity or an extreme inflow flood exceeding the design capacity may lead water flowing over a part or the entire length of the dam. Subsequently, erosion begins on the downstream face of the dike due to the excess tractive shear stress.

Reliable measurements of the breach evolution and overtopping flow discharge at laboratory scale remains limited due to several factors which are difficult to carefully control such as the supercritical flow condition on the downstream slope, its shallowness, the rapid change of bathymetry and surface flow elevation, and in the slope-infiltration of the downstream face of the embankment. During the past twenty years, various techniques have been used to evaluate the overtopping breach hydrograph. For example, the hydrologic routing algorithm (Al-Riffai and Nistor 2013), broad-crested weir formula (SINGH 1996), circular-crested weir formula (Schmocker and Hager 2010), and V-notch weir at the channel end (Pickert, Weitbrecht and Bieberstein 2011); (Coleman, Andrews and Webby 2002).

The purpose of this study is to present a novel technique for evaluating the direct breach hydrograph at the crest of a non-cohesive soil embankment using an improved particle tracking velocimetry approach that uses proper LED black lighting with fluorescent particles, high-speed and high spatial resolution Phantom cameras, and an improved surface velocity measurement technique during overtopping flow. Visualizing flow and capturing both bed and surface flow profiles with a high degree of resolution was achieved by injecting an appropriate amount of fluorescent dye and tracing its movements over and through the body of the embankment.

2 EXPERIMENTAL SETUP

The embankment breaching experiments were conducted in the elevated flume in the Hydraulic Laboratory at the University of Ottawa. The flume was 12.2 m long, 0.385 m wide, 0.60 m height and bounded laterally by glass side walls as shown in Figure 1. The flume bottom was horizontal and impervious and a raised PVC floor 0.05 m thick was inserted to add bottom drainage at a distance of 1.616 m from its outlet downstream end. Bottom drainage was designed such that it allowed for a sufficient seepage discharge capacity and it was interchangeable for different embankment geometry configurations. Seepage water was collected and channeled to the drainage tank through twelve identical hoses of 25 mm diameter. A total of four WG-50 capacitance wave gauges and two mPulse ultrasonic sensors were used to measure the time-history of water surface elevations with a sampling rate of 30 Hz. Two wave gage WG-50s sensors were installed in the upstream reservoir and at the embankment location, while other two WG-50s were installed in the outlet and seepage tank. Two high-speed Phantom 410L cameras with a recording capacity of 1000 fps was installed above and at the side of the embankment model along with a GoPro camera used for a far field of view. Green fluorescent dye was injected with a dilution of 1 ppm to visualize the flow and improve the contrast of photographic images. Styrofoam balls (2-3) mm size painted with fluorescent color were used as a tracing particle to measure flow surface velocity during overtopping.

An LED blacklight system was installed on the downstream side of the embankment to illuminate the fluorescent particles and visualizing the flow. The volume of the water at the reservoir was controlled and set constant throughout all tests using a Plexiglas vertical wall. To control the light reflection and enhance the blacklight effect, the entire test facilities covered with a light-impermeable tarp as shown in Figure 2. Micro- tensiometer-transducer probe assemblies (MTTPA) were installed on left side of the embankment to measure time-history pore-water-pressure inside the body of the embankment.

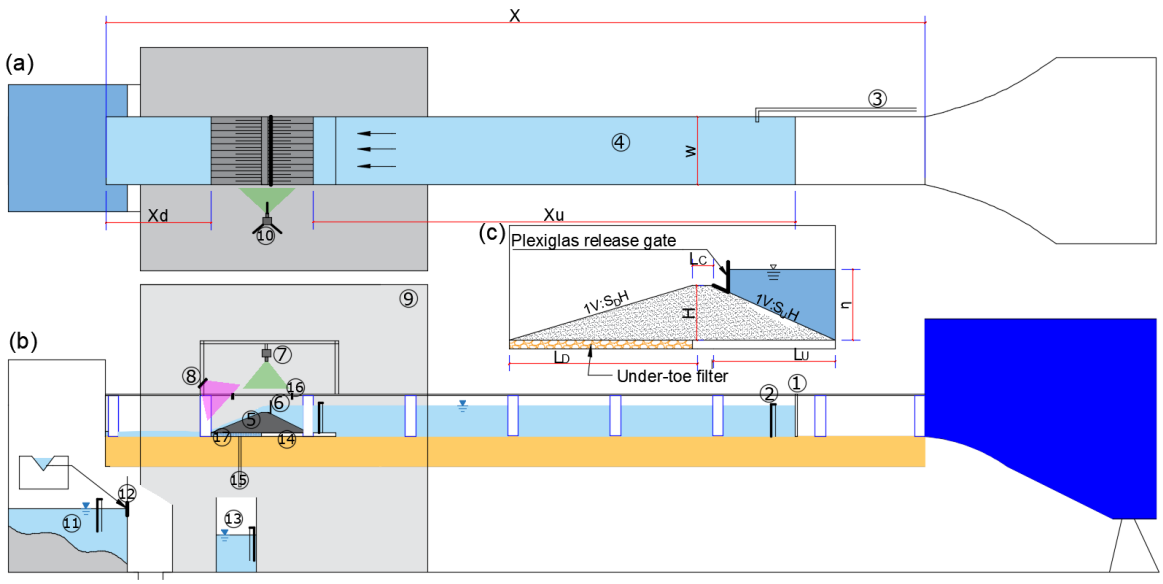

Figure 1: Embankment Breach Setup with (a) top view and (b) side view with,(c) Embankment section; (1) U/S wall, (2) WG-50, (3) Inlet water supply , (4) Reservoir, (5) Embankment, (6) Release gate, (7) Overhead HSPC ,(8) LED Blacklight, (9) Tarp, (10) Side HSPC, (11) Outlet tank, (12) V-notch, (13) Seepage tank, (14) False floor, (15) Drainage, (16) sensors, (17) Under toe filter, X = 12.2 m, Xu = 7.08 m, Xd = 1.61 m, W = 0.385 m

Figure 2: Experimental flume: left photo: flume covered with the tarp; right photo: a model of the embankment with LED light on

The embankment models were a trapezoidal shape with H = 0.3 m high. The crest was Lc = 0.1 m wide, upstream toe length L_U = 0.75 m long, downstream toe length L_D = 0.6, 0.9, 1.2 m long, and the upstream and downstream face slopes were S_U = 1V:2.5H and S_D = 1V:(2, 3, 4) H, respectively. To minimize the effect of tailwater on the erosion of downstream toe and slope, the models of the embankments were constructed near the flume outlets as shown in Figure 1. To avoid sliding failure due to seepage and control sub-surface flow, bottom drainage was added underneath the entire downstream toe as shown in Figure 1c.

A series of geotechnical tests were conducted on embankment material samples in the Geotechnical Engineering Laboratory at the University of Ottawa prior to construction and testing. These included the dry

unit weight (looses and compacted), $\gamma_{dmin}\ and\ \gamma_{dmax}$, minimum and maximum porosity, $e_{min}\ and\ e_{max}$ (ASTM D4254 -16), sieve analyses,D_{50}, coefficient of curvature, C_C, uniformity, C_U, standard deviation, σ_S (ASTM D422 -16), angle of internal friction,ϕ' (ASTM D854 06e1), specific gravity, G_S (ASTM D3080 -04), constant head permeability test, K_{sat} (ASTM D2434 -68), angle of repose in dry and saturated condition,Ψ (Frank 2016), and soil-water-characteristic-curve SWCC using standard temple cell apparatus, $AEV\ and\ RSV$ (ASTM D2325 -68). Summaries the results and analysis are listed in Table 1

Table 1: Characteristic sediment properties

d_{10} (mm)	d_{30} (mm)	d_{50} (mm)	d_{60} (mm)	d_{90} (mm)	C_C	C_U	σ_s	γ_{dmin} (kN/m^3)
0.40	0.46	0.5	0.52	0.59	1.02	0.75	1.32	15.0
γ_{dmax} (kN/m^3)	e_{min}	e_{max}	K_{sat} (cm/s)	G_s	ϕ' (deg.)	Ψ (deg.)	AEV (kPa)	RSV (kPa)
17.0	0.422	0.344	0.812	2.64	40.6	32.2	2.0	2.9

† AEV (air entry value), RSV (residual suction value), Ψ (angle of repose), ϕ'(angle of internal friction)

To investigate the impact of embankment geometry element (downstream slope), three different slopes (1:2, 1:3, 1:4) were tested. While the upstream slope remained unchanged for all three configurations. The hydraulic boundary condition for the upstream reservoir was falling head with an initial head of 5 cm and 10 cm above the crest of the dam. A Plexiglas release gate was installed on the upstream face of 13 cm away from the crest. Once the water level reached the desired level, the gate was released, and the breaching process triggered. Table 2 shows the testing program for the present study.

Table 2: Test program for the present study

Test	Downstream Slope	Upstream Slope	Crest length and height (cm)	Initial Head (cm)	comment
T01	1V:3H	1V:2.5H	10, 30	5	
T02	1V:3H	1V:2.5H	10, 30	10	
T03	1V:3H	1V:2.5H	10, 30	10	Same as T02 for repeatability
T04	1V:2H	1V:2.5H	10, 30	5	
T05	1V:2H	1V:2.5H	10, 30	10	
T06	1V:4H	1V:2.5H	10, 30	5	

3 MEASUREMENT TECHNIQUES

Prior to each test, all four-wave gauges, sensors, and tensiometers were calibrated and stored properly as shown in Figure 3. The reservoir was filled up to the desired level (35 and 40 cm) from the bottom of the embankment using 12 mm hose. The reservoir level was monitored during the falling state, as a result of overtopping flow after releasing the Plexiglas release gate, using two WG-50 wave gauges with a sampling

frequency of 30 Hz. WG-1 installed at the beginning of channel and WG-2 at the u/s toe of the dam. In addition to two ultrasonic sensors, S1 at mid of u/s slope and S2 at d/s slope to measure water surface level. WG-3 was installed at the outlet tank to measure the head above the V-notch, and WG-4 was installed in the volumetric tank to evaluate seepage flowrate. WG1 and WG2 were used to evaluated breach hydrograph using hydrologic routing technique as per Eq.1, while the WG3 was used to measure the outlet flowrate using a 90° V-notch formula Eq. 2. The data acquired from WGs were filtered to reduce the noise using Matlab Butterworth filter algorithm.

[1] $$\sum Q_I - \sum Q_O = \frac{\Delta V}{\Delta t}$$

where Q_I is inflow discharge in (l/s) and in the present study is equal to zero, Q_O is outflow discharge in (l/s) and here is breach discharge, ΔV is V2-V1 change in reservoir volume over a differential time step Δt.

[2] $$Q_O = C_W \Delta h_W{}^{2.5}$$

where C_W is a coefficient of discharge based on weir shape, (for 90° triangular is 1.38) and Δh is the head above the V-notch apex.

Figure 3: Calibration Process: left photo - tensiometers; right photo - wave gauges

The real-time pore-water-pressure inside the body of the embankment were measured using eighteen micro-tensiometer-transducer probe assemblies (MTTPA), assembled and calibrated before use in the experiment. The MTTPA utilized porous ceramic probes of 2 mm in diameter and 20 mm length as shown in Figure 4 .The MTTPA sensors capable of measuring both positive and negative gauge/differential pressure (± 7 kPa) (Al-Riffai and Nistor 2013), which is adequate for capturing both saturated and unsaturated pore water pressure in the above laboratory embankment model.

The novel approach was consisting of two high-speed phantom cameras with a sampling frequency of 1000 Hz. These cameras provide high temporospatial resolutions, which is necessary for a high flow velocity field and erosion rate. Fluorescent painted Styrofoam balls of (2-3) mm diameter used as seeding particles. Those particles were used in feeding the flow continues at some distance upstream of the embankment to provide tracing and as a result surface velocity through the breaching process. Before the construction of the embankment model, both cameras installed above and at the right side of the experiment section. The fluorescent chessboard was used to calibrate both cameras by placing horizontally at the bottom and at the height of initial reservoir level to calibrate the top camera, while the calibration sheet placed vertically at front and back of the flume glasses for calibrating the side looking camera. Each square of the sheet shown in Figure 5 represents the 40 mm dimension. All wave gauges, tensiometers, and cameras were synchronized together using National Instrument NI data acquisition. LabVIEW was used to program and

trigger the measuring devices. A five-second delayed time was set for the cameras, which means that all sensors will start recording 5 seconds before the cameras and this was decided to save the memory of the cameras and start firing at the time release gate lifted. Images from top camera rectified, calibrated, scaled and processed in Davis 8.4.0 by applying a various filter to enhance the imaging quality, object detection and eliminating noises as shown in Figure 6. In order to calculate the breach discharge at the crest of the embankment, the surface velocity extracted from the velocity field at the points where the position of the particle at the cross-section line then average value was taken. Corresponding to the same line where velocity obtained, the water depth was extracted from the images acquired from side camera after processing in the Phantom PCC software and georeferencing in QGIS to the same instant time of the surface velocity.

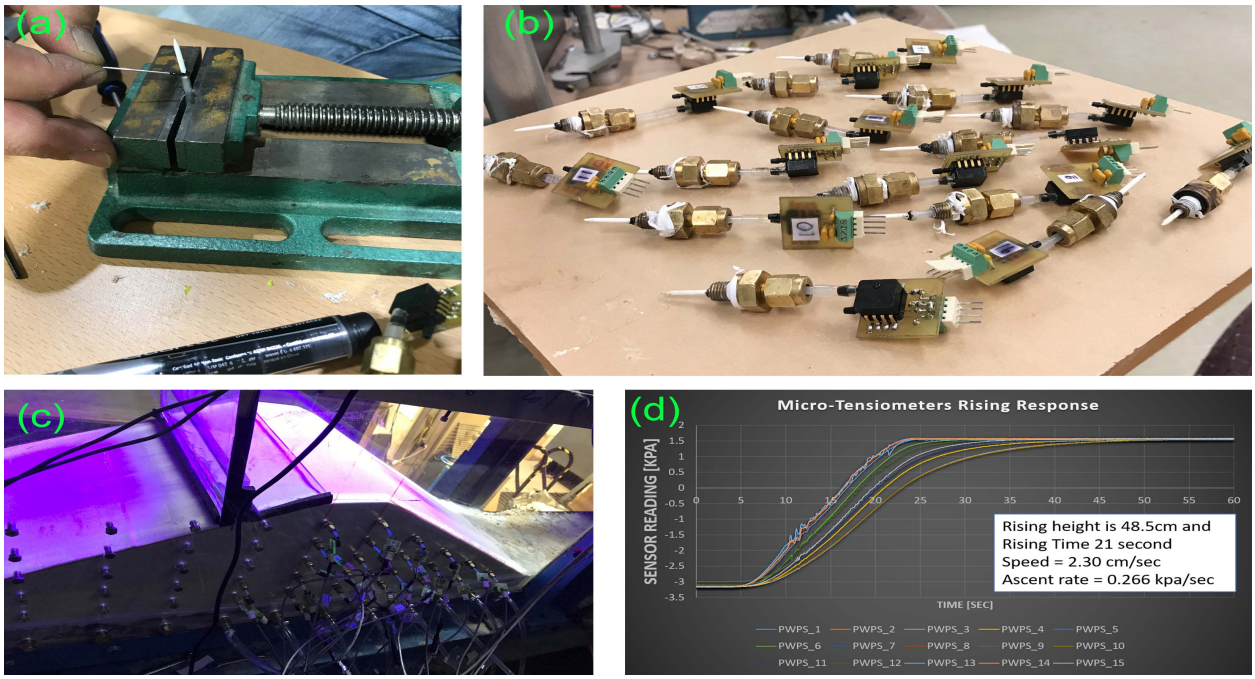

Figure 4: Pore-pressure micro-tensiometers: assembly, installation, and response time for rising head

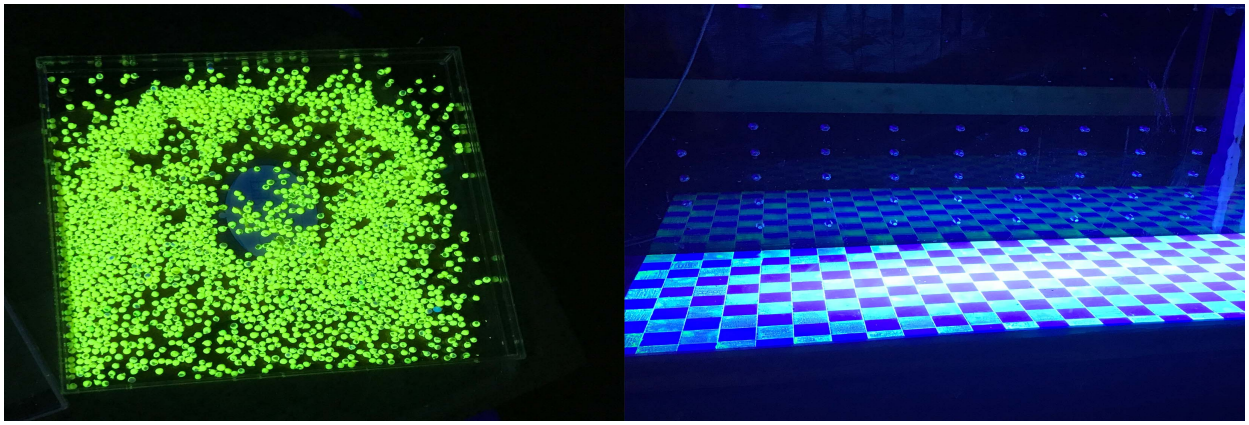

Figure 5: Left photo: seeding particles; Right photo: calibration sheet

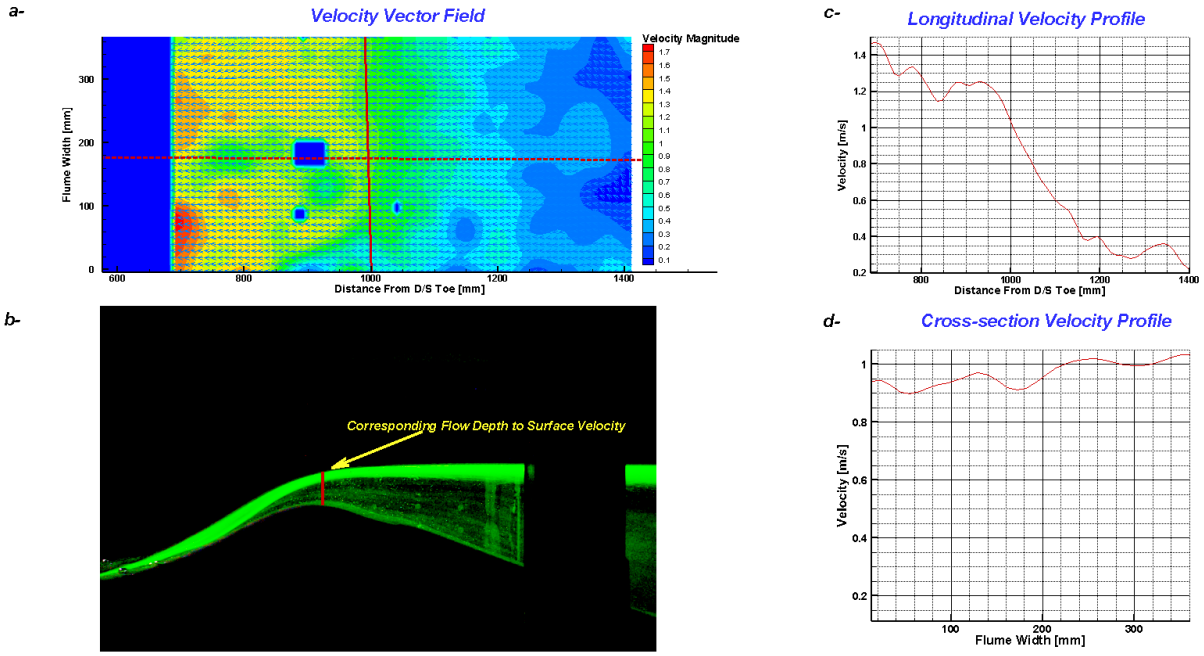

Figure 6: Instantaneous surface velocity at instant t = 8.2 second

4 DISCUSSION OF RESULTS

4.1 Breach Evolution

In order to understand the breach mechanism and sediment erosion on steep-slope and under supercritical flow as occurred on downstream slope of embankment failure due to overtopping flow, it is essential to obtaining an accurate bed and surface flow profile. Figure 7 shows the bathymetry change with the breach progress. It is worth noting that the discontinuity of bed profile near the d/s toe of the embankment because of the strong erosion and entrainment of sediment into the flow. However, the water surface profile for the entire field of view of the side camera extracted as appears in Figure 7b.

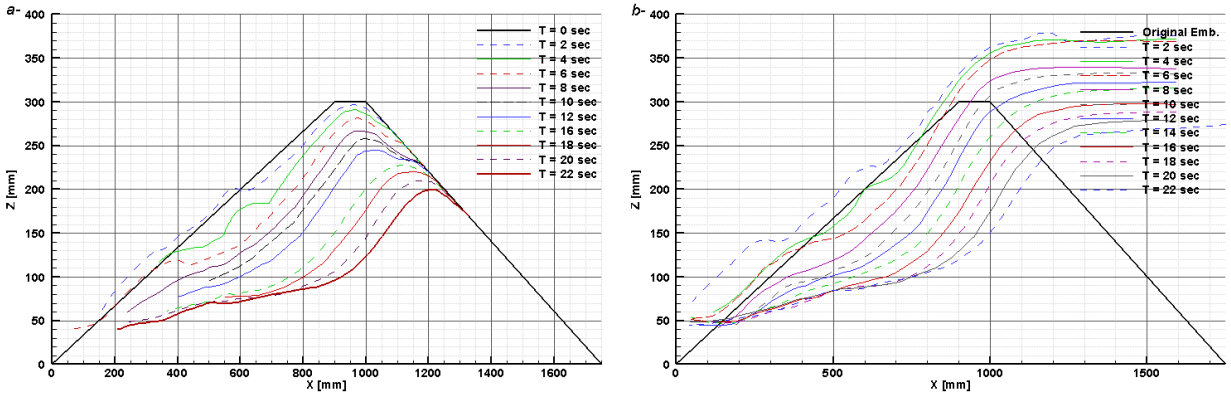

Figure 7: a) embankment breach profile; b) overtopping flow profile, for test T02 at various times T

An additional feature of the present study result was quantifying the breach hydrograph properly. Therefore, the outcome of the novel PTV technic was used to produce overtopping flowrate at the crest of the dam. The advantage of this method over the previously used methods was overcoming the challenges in a direct

measurement. For instance, the disadvantage of hydrologic flood routine was ignoring the seepage through the upstream face of the embankment, and improper measurement of reservoir drawdown due to non-linearity of surface flow specifically near the upstream crest. Moreover, the shape of the crest for such a model was not circular. This means that this method is not valid. Sedimentation and flowing mixture of sand and water together in addition to the distance and backwater effect, choice of using V-notch weir at the end of the channel was not appropriate. These considerations imply that the PTV as mentioned earlier approach was applicable. Figure 8 shows different methods of predicting breach hydrograph for test T02.

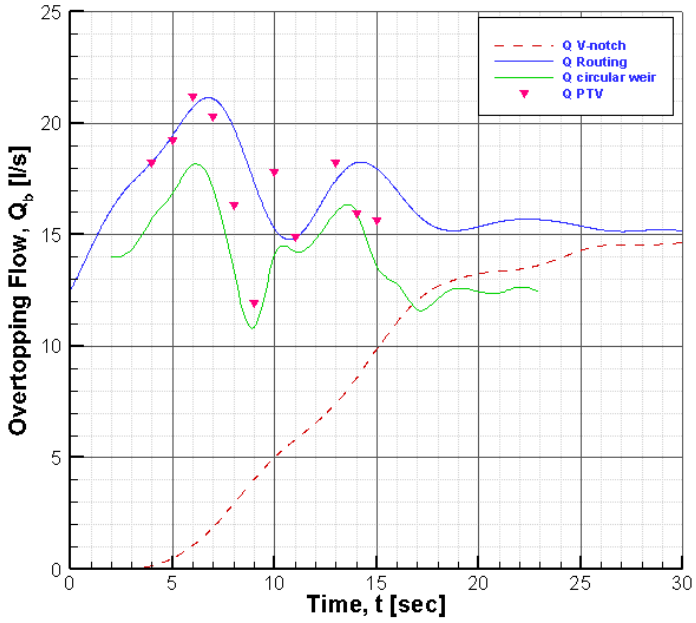

Figure 8: Breach hydrograph for test T02

Embankment breach is a complex phenomenon. For instance, infiltration on the downstream slope may affect the erosion process. According to (LIU and CHIEW 2012), the downward seepage on sediment transport on horizontal bed flume tests shows that suction influence bed shear stress, critical shear stress and eventually bed-load transport rate. Thus, the recorded data from tensiometers combined with the pressure head of surface flow on the bed and considering the curvilinear flow, mapped using ArcGIS tool. For instance, Figure 9 shows the sub-surface flow analysis during a breach event.

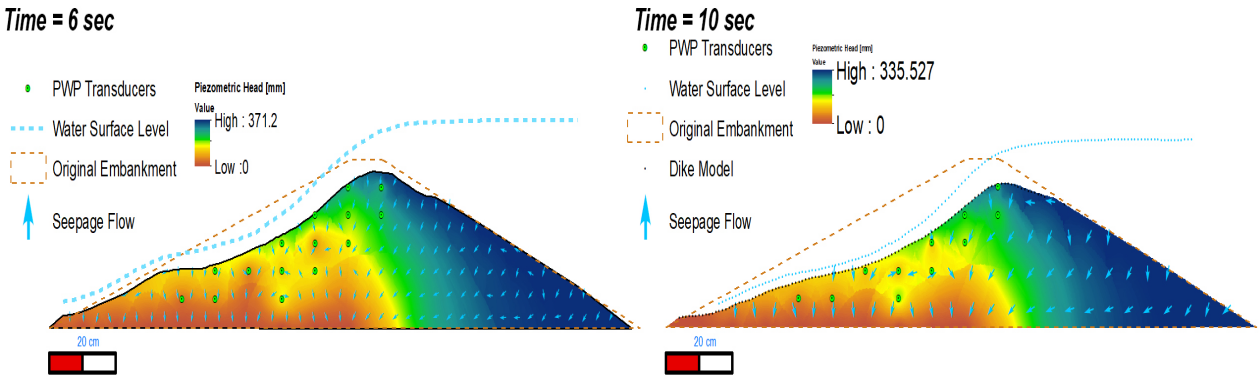

Figure 9: PWP interpolation and seepage analysis for test T02 at time T = 6 and 10 sec

4.2 Effect of Downstream Slope and Overtopping Head

The effect of the downstream slope and overtopping head on breach process and consequently the outflow hydrograph was investigated. The hydrographs (Figure 10) computed for the three embankment configurations indicated that erosion rate (Figure 11) for steeper slope under the high initial overtopping head (10 cm) is quite faster due to the acceleration of flow and high shear stress applied on the bed material. In contrast, with the low initial overtopping head (5 cm), the downstream slope has less impact on peak-flow rather than delaying the erosion progress.

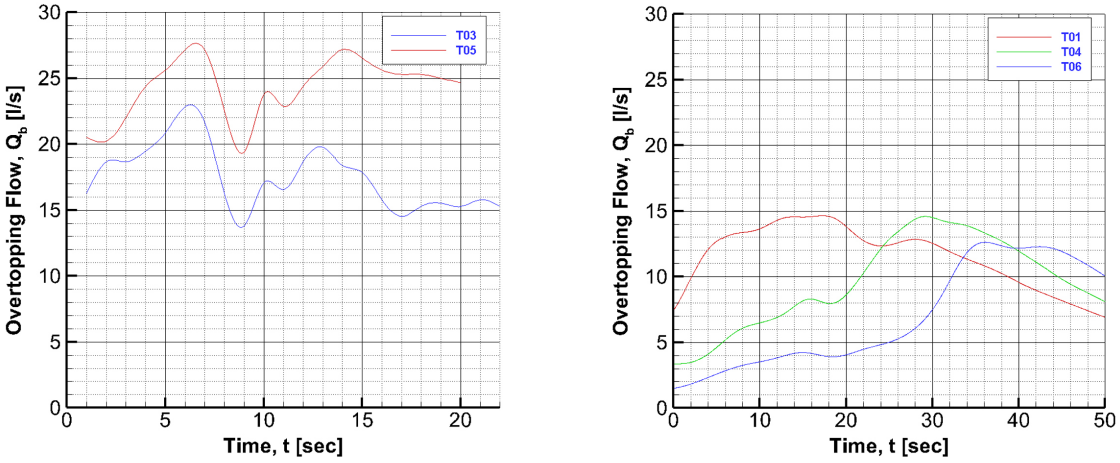

Figure 10: Breach outflow hydrograph, right plot: low overtopping head; left: high overtopping head

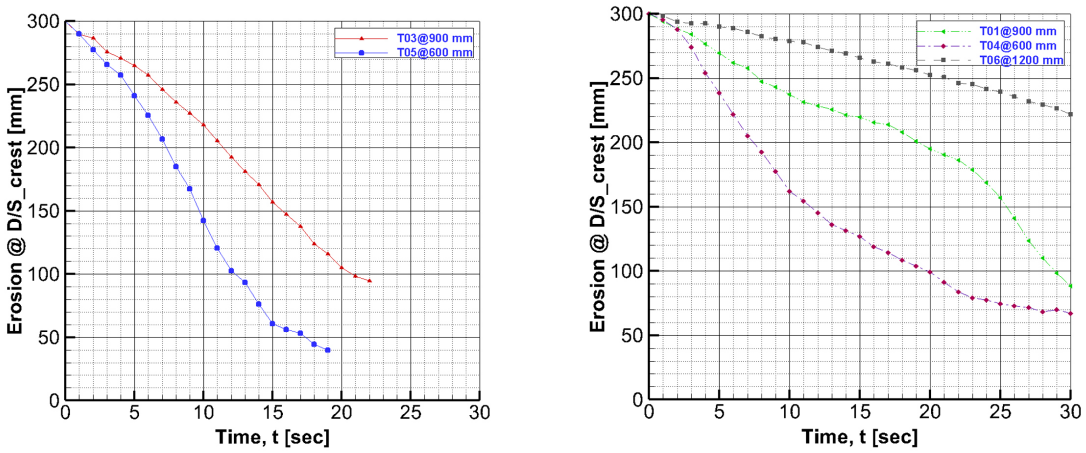

Figure 11: Erosion Rate : Left plot: low overtopping head; right plot: high overtopping head

ACKNOWLEDGMENTS

The authors would like to thanks Dr.Mahmoud Al-Riffai for guidance on assembling MTTPs and useful equipment he left after his research work at the University of Ottawa. The authors would like to appreciate the efforts of the officers, Mark, Leo, and Jean-Claude, from Hydraulic, Electrical and Geotechnical

departments for preparation of the experiments. The assistance of Marieh Rajaie a Ph.D student at the University of Ottawa, and an internship student: Antoine, Gabriel and Pierre greatly appreciated.

REFERENCES

Al-Riffai, M. and Nistor, I. 2013. "Influence of boundary seepage on the erodibility of overtopped embankments: A novel measurement and experimental technique." *Proceedings of 2013 IAHR Congress,* Tsinghua University Press, Beijing.

ASTM D2325. -68. *Standard Test Method for Capillary-Moisture Relationships for Coarse- and Medium-Textured Soils by Porous-Plate Apparatus .* West Conshohocken: ASTM International.

ASTM D2434. -68. *Standard Test Method for Permeability of Granular Soils (Constant Head).* West Conshohocken: ASTM International.

ASTM D3080. -04. *Standard Test Method for Direct Shear Test of Soils Under Consolidated Drained Conditions.* West Conshohocken: ASTM International.

ASTM D422. -16. *Standard Test Method for Particle-Size Analysis of Soils.* West Conshohocken: ASTM International.

ASTM D4254. -16. *Standard Test Methods for Minimum Index Density and Unit Weight of Soils and Calculation of Relative Density.* West Conshohocken: ASTM International.

ASTM D854. 06e1. *Standard Test Methods for Specific Gravity of Soil Solids by Water Pycnometer.* West Conshohocken: ASTM International.

Coleman, S.E., Andrews, D.P. and Webby, M.G. 2002. "Overtopping breaching of noncohesive homogenous embankments." *Journal of Hydraulic Engineering,* **189**(9): 829-838.

Frank, P-J. 2016. "Hydraulics of spatial dike breaches." Ph.D. Thesis, Swiss Federal Institute of Technology (ETH) Zurich university, Zurich, Switzerland.

Liu, X.X., and Chiew, Y-M. 2012. "Effect of Seepage on Initiation of Cohesionless Sediment Transport." *Acta Geophysica,* **60**(6): 1778-1796.

Pickert, G., Weitbrecht, V., and Bieberstein, A. 2011. "Breaching of overtopped river embankments controlled by apparent cohesion." *Journal of Hydraulic Research,* **49**(2): 143-156.

Rifai, I., Erpicum, S., Archambeau, P., Violeau, D., Pirotton, M., Abderrezzak, K.E.K., and Dewals, B. 2017. "Overtopping induced failure of noncohesive, homogeneous fluvial dikes." *Water Resources Research*, **53**(4): 3373-3386.

Schmocker, L., and Hager, W.H. 2010. "Overtopping and breaching of dikes - Breach profile and breach flow." *Proc. Intl. Conf. River Flow,* Braunschweig, Germany: A. Dittrich, K. Koll, J. Aberle & P. Geisenhainer, eds. 515-522.

Schmocker, L., Halldórsdóttirm, B.R. and Hager, W.H. 2011. "Effect of Weir Face Angles on Circular-Crested Weir Flow." *Journal of Hydraulic Engineering,* **137**(6): 637-643.

Singh, V.Y.P. 1996. *Dam breach modelling technology.* Springer Science+Business Media Dordrecht.

Visser, P.J., Zhu, Y., and Vrijling, J.K. 2006. "Breaching of dikes." *30th Int. Conf. Coastal Engineering,* San Diego CA. 2893-2905.

Zhang, L., Peng, M., Chang, D.and Xu, Y. 2016. *Dam Failure Mechanisms and Risk Assessment.* John Wiley & Sons Singapore Pte. Ltd, Singapore.